Novel Ways to Determine Kinesin-1's Run Length and Randomness Using Fluorescence Microscopy

Sander Verbrugge, Siet M. J. L. van den Wildenberg, and Erwin J. G. Peterman*
Department of Physics and Astronomy and Laser Center, VU University, Amsterdam, The Netherlands

ABSTRACT   The molecular motor protein Kinesin-1 drives intracellular transport of vesicles, by binding to microtubules and making hundreds of consecutive 8-nm steps along them. Three important parameters define the motility of such a linear motor: velocity, run length (the average distance traveled), and the randomness (a measure of the stochasticity of stepping). We used total internal reflection fluorescence microscopy to measure these parameters under conditions without external load acting on the motor. First, we tracked the motility of single motor proteins at different adenosine triphosphate (ATP) concentrations and determined both velocity and (for the first time, to our knowledge, by using single-molecule fluorescence assays) randomness. We show that the rate of Kinesin-1 at zero load is limited by two or more exponentially distributed processes at high ATP concentrations, but that an additional, ATP-dependent process becomes the sole rate-limiting process at low ATP concentrations. Next, we measured the density profile of moving Kinesin-1 along a microtubule. This allowed us to determine the average run length in a new way, without the need to resolve single-molecules and to correct for photobleaching. At saturating ATP concentration, we measured a run length of 1070 ± 30 nm. This value did not significantly change for different ATP concentrations.

INTRODUCTION

Kinesin-1 is a motor protein that drives intracellular transport of vesicles and organelles in many eukaryotic organisms (1). To fulfill this task, Kinesin-1 (called ''kinesin'' hereafter) steps along microtubules (MTs), with a step size of 8 nm (2,3). Each step is driven by the hydrolysis of one adenosine triphosphate (ATP) molecule into adenosine diphosphate (ADP) (3). Both kinesin's velocity and ATPase rate are dependent on the ATP concentration and follow Michaelis-Menten kinetics (4). Kinesin has two identical motor domains that transiently bind to the MT and contain the active site for ATP-hydrolysis. These two motor domains are kept out of phase, and thus, work together such that the motor domains can make hundreds of processive steps along the MT (5).

Over the last years, the technical approaches that allow for the resolution of single steps have tremendously increased our insight in kinesin's mechanism. Optical trapping experiments have taught us that kinesin's center-of-mass makes 8-nm steps at an average step time of ~10 ms (at saturating ATP concentration) (2), that one ATP molecule is hydrolyzed per step (3), and that kinesin slows down when a load is applied and stalls at a counteracting force of ~5 pN (2,5). Single steps have also been discerned in wide-field optical microscopy experiments. Traveling-wave tracking (6) has allowed for determination of step sizes and rates with microsecond time resolution and subnanometer spatial-resolution without external load (7). In wide-field fluorescence micros-

copy, a localization accuracy of several nanometers has been achieved by fitting the point-spread function (8–10). This approach has been applied to kinesin with a fluorescent label attached to only one of the motor domains, directly demonstrating that each individual motor domain makes steps of 16 nm (11), confirming that the motor domains move in a hand-over-hand fashion (12,13).

Although these techniques have provided fundamental insight in kinesin's stepping mechanism, many key properties of motor motility do not require the resolution of single steps and can thus be determined faster, with less complex and more widely available instrumentation. This is important in light of the many motor proteins that have been studied to a lesser extent than Kinesin-1, such as dynein and Eg5 (14,15), or numerous others that have not been studied at all on the single-molecule level. We see, in particular, three parameters as important for defining a motor protein's motile properties: the run length, the velocity, and the so-called randomness (3). Each of the three is a function of ATP concentration.

The run length is the average distance a motor protein travels along its track before it releases, and this describes the processivity of a given motor protein. The run length is, in most cases, measured using wide-field, single-molecule fluorescence microscopy on labeled motors. For kinesin, typical values of ~1 μm (depending on the exact conditions) have been obtained, indicating that it makes >100 8-nm steps before it releases from the MT (16,17). Single-molecule fluorescence measurements of the run length are complicated by photobleaching of the fluorophores, which requires a correction of the measured run length for photobleaching and hence determination of the fluorophore bleaching rate. Here, we demonstrate another way of determining the run length using total internal reflection fluorescence (TIRF)

---

microscopy that does not require the observation of single motors and can thus be performed under illumination conditions at which photobleaching is negligible. In our approach, we measure the fluorescence of many motors walking along an MT, and derive the run length from the motor-concentration profile on the minus-end of the MT.

The velocity of a motor protein is another key motility parameter. The two most widely applied approaches to measure the velocity of a kinesin are surface-gliding assays and single-motor walking assays, detected with single-molecule fluorescence. The former approach is a multimotor assay, in which the motors are bound to a surface, and the motility of the MT track driven by these bound motors is measured using fluorescence or other microscopy methods (4). In the latter, single-molecule approach, the MTs are bound to the surface and the motion of single motors is followed (1,2,18). Although it requires a more-advanced instrumentation, we have a preference for the latter method; because it allows for monitoring of the multimeric state of the motor proteins, it is less prone to undesired interactions with the surface, and can resolve potential heterogeneous behavior. By performing the measurements at different ATP-concentrations, the Michaelis-Menten parameters can be obtained. These parameters describe the intrinsic catalytic rates and the affinity of the active site for ATP. Typically, for Kinesin-1, a maximum velocity at ~900 nm s^{-1} and a K_m (the substrate concentration at which half the velocity is reached), at ~30 μM, has been determined (19).

The randomness of motility (r) of a motor protein can be obtained from time-displacement trajectories ($x(t)$) of individual motors using Eq. 1 (20), once the step size, s, is known,

$$r = \lim_{t \to \infty} \frac{\langle\langle x(t)^2\rangle - \langle x(t)\rangle^2\rangle}{s\langle x(t)\rangle} = \frac{1}{s}\frac{1}{v}\frac{d\langle\langle x(t)^2\rangle - \langle x(t)\rangle^2\rangle}{dt},$$

(1)

with v the velocity of the motor. The randomness is a measure of the stochasticity of the time between steps (dwell time). If the motor were to be a perfect clock (i.e., the duration between steps would be constant), there would be no variance in the dwell times and therefore the randomness would be zero. If, on the other hand, the stepping would be determined by a single exponentially distributed, rate-limiting process, the randomness would be one. In the case of two sequentially occurring, exponentially distributed processes, with, on average, equal duration, the randomness would be one-half. For Kinesin-1, the randomness has been measured using traveling-wave tracking (6) and optical tweezers (3,20,21). In the most elaborate studies using optical tweezers, at different ATP concentrations and a load of 1.05 pN (21), it was found that the randomness is approximately one-half at saturating ATP, decreases with ATP-concentration to one-third (at ~K_m), and then increases to one at even lower ATP-concentrations. This behavior was explained by Kinesin-1's mechanism consisting of two rate-limiting, ATP-concentra-

tion-independent exponential processes and one ATP-dependent process. At lower ATP-concentrations, ATP-binding takes longer and longer, first leading to a decrease of the randomness (three processes become rate-limiting) and subsequently, at concentrations below K_m, to an increase to unity (only ATP-binding is rate-limiting). In a later study, a more complex data set, involving force dependence of the randomness, was described with a more elaborate model. This involved five states, including one reversible ATP-concentration dependent and one reversible ATP-independent transition. Of these transitions, four were required to be force-dependent. Here, we show that the randomness of kinesin motility can also be measured using single-molecule fluorescence microscopy—which has the advantage of less complicated, more widely available instrumentation, and of enabling measuring without applying a load to the motor. Our data can be well described based on models with one ATP-dependent rate and at least two additional ATP-independent rates.

MATERIALS AND METHODS

Experimental setup

Assays were performed at 21°C using an epi-illuminated wide-field fluorescence microscope. Excitation light was coupled into a TIRF-objective (TIRF Plan Apo 100×/1.45 oil; Nikon, Amstelveen, The Netherlands) with a polychromatic dichroic mirror (Z488RDC/532/633RPC; Chroma, Rockingham, VT) that allowed for combined excitation with a 635-nm (IQ1C10(LD1338)G3H5; Power Technology, Little Rock, AR) and a 532-nm laser (Compass 215M-20; Coherent, Santa Clara, CA). To induce TIRF, the excitation beam was coupled off-axis into the objective creating an evanescent wave in the sample. Fluorescence was collected with the objective and filtered using HQ610/75M or a HQ700/75M bandpass filter (Chroma). The two spectral bands were imaged sequentially on a charge-coupled device camera (MicroMax 512FTB; Princeton Instruments, Trenton, NJ).

Microtubule preparation

Tubulin was purified from pig brain and labeled with Cy5 (14); biotinylated tubulin was purchased (027T333-A; Cytoskeleton, Denver, CO). To polymerize MTs, tubulin was incubated in PEM80 (80 mM H$_2$PIPES, 1 mM EGTA, and 2 mM MgCl$_2$, pH 6.8, adjusted with NaOH) with GMPCPP (200 μM, Jena Bioscience, Jena, Germany) at 37°C for 20 min. Subsequently, the MTs were stabilized with 10 μM Taxol and stored at room temperature.

Experimental assay for kinesin density profile determination

To determine the motor density profile along a MT, a chamber was prepared by attaching plasma-cleaned dimethyl-dichlorosilane-treated slides to coverslips using double-stick tape. The chambers were incubated for 5 min with bovine-serum albumin-biotin at 0.1 mg mL^{-1} (A2289; Sigma-Aldrich, Zwijndrecht, The Netherlands) in PEM80, washed with buffer and incubated for 5 min with streptavidin at 0.1 mg mL^{-1} (8587, Sigma-Aldrich). The surface was blocked by incubating with 0.2% (w/v) Pluronic F108 (BASF, Ludwigshafen, Germany) for 5 min. Next, the chamber was incubated with biotinylated Cy5-labeled MTs for 5 min. After rinsing with buffer, the chambers were flushed with Alexa555-labeled kinesin at a concentration of roughly 20 nm. Truncated human kinesin of 391 amino acids with a single surface-exposed cysteine at amino-acid position 217 (hKin391-T217C) was used,

a kind gift from Günther Woehlke, Technical University of Munich, Munich, Germany. The labeling stoichiometry was ~1 Alexa555/kinesin dimer, determined from the absorbance ratio at 280 nm and 555 nm in motility buffer containing PEM80 with 4 mM dithreitol, 25 mM glucose, 20 μg mL^{-1} glucose oxidase, 35 μg mL^{-1} catalase, ATP, and an ATP-regeneration system, added as previously described (22). The exposure time during the measurements of the motor density on the MT was 1 s and the excitation power was 9 μW (>10 times lower than the power required for single-molecule imaging). To obtain an intensity profile of many kinesin motors on a single MT, >100 frames were averaged. Stacks of images were acquired using Winview (Princeton Instruments) and analyzed with routines written in Labview 8.2 (National Instruments, Austin, TX).

Experimental assay for velocity and randomness determination

Coverslips were plasma-cleaned for 20 min. A positively charged surface was created by amino-silanization with 3-[2-(2-aminoethylamino)ethyl-amino]-propyl-trimethoxysilane (DETA; Aldrich). Sample chambers were first incubated with Cy5-labeled MTs followed by 5 min incubation with 0.2 mg mL^{-1} casein. Next, the chambers were flushed with Alexa555-labeled kinesin at a concentration below 1 nM in the motility buffer. In these experiments, a truncated (at amino acid 560) human kinesin construct containing only a single native cysteine residue at position 421 (hKin560-421C) was used. At 4 μM ATP, an ATP-regeneration system was added.

Calculation of velocity and randomness

From stacks of images, traces were extracted using kymographs as described elsewhere (14). A trace was defined as the discretely sampled trajectory of a single motor between appearance and disappearance of a fluorescent spot on a MT. The x-y coordinates of a moving spot were determined by fitting a two-dimensional Gaussian to the observed fluorescence intensity profile in each frame (9). Only traces with a minimum length of three time points were used. In the rare event that a motor stalled, traces were discarded or only the beginning segment was used. The mean displacement ($MD(\tau)$) was calculated from the traces for all independent (nonoverlapping) time lags (τ) in all trajectories at a given ATP concentration. The error was estimated by calculating the standard error of the mean. The motor velocity, at each ATP concentration, was determined from a weighted linear fit to $MD(\tau)$ ($MD(\tau) = v\tau$). Next, the variance of the MD(var(τ)) was calculated for each time lag (τ) with var(τ) = $\langle x^2(\tau) \rangle - \langle x(\tau) \rangle^2$. The error was estimated by calculating the standard error of the mean. The variance of the mean displacement at a certain time lag has a time-dependent contribution due to the randomness of stepping (20) and a time-independent offset due to the localization uncertainty of fluorescent spots (23). The offset was approximately constant in all experiments (540 $\pm$ 30 nm^2), implying a localization uncertainty of ~23 nm. The randomness (Eq. 1) was determined by a weighted linear fit to the variance at the first 10 time lags (corresponding to a traveled distance of ~130 nm (24)) for every ATP concentration.

Modeling the ATP-concentration dependence of the randomness

The ATP-concentration dependence of the randomness was modeled with three distinct models (3). All three consist of a single ATP-concentration-dependent process (that dominates at low ATP concentrations). The duration of this process (T_{ATP}) is calculated using $T_{ATP} = K_m/k_{cat}[ATP]$), with $k_{cat} = v_{max}/s$ and K_m the Michaelis-Menten parameters determined in the velocity experiments. The three models differ in the number of ATP-independent exponential processes: 1, 2, or 3, all with the same duration, $T_n = 1/(nk_{cat})$ (with n representing the number of additional ATP-independent processes). The randomness is then calculated using

$$ r = \left(\frac{T_{ATP}}{T_{tot}} \right)^2 + \sum_{i=1}^{n} \left(\frac{T_i}{T_{tot}} \right)^2, $$

with

$$ T_{tot} = T_{ATP} + \sum_{i=1}^{n} T_i = \frac{K_m}{k_{cat}[ATP]} + \frac{1}{k_{cat}} $$

as the total stepping time.

In addition to these three models, we compared our data to a fourth, more complex model consisting of five states (25), the first transition being ATP-dependent and only the first and second transitions being reversible. This reaction scheme was modeled using stochastic simulation (100,000 transitions, and the transition times were obtained from exponential distributions with fixed transition rates). The values for k_{cat} and K_m used by Block et al. (25) differ from the values we observed, which might reflect the different source of the protein (human versus squid). To account for this, we adjusted the transition rates in the five-state model to fit our Michaelis-Menten parameters, while keeping the ratios the same. Note that all models applied do not contain fitting parameters.

RESULTS

Determination of kinesin's velocity and randomness using TIRF microscopy

To determine the randomness of Kinesin-1's motility at zero load using TIRF microscopy, we tracked single, fluorescently labeled kinesin motors binding to and moving unidirectionally along MTs (Fig. 1). The illumination conditions were optimized for signal/noise and an average displacement of, at most, 20 nm was allowed within the integration time of one frame. From stacks of images obtained in this way (Fig. 1 b), time trajectories of individual kinesin motors (position as function of time) were extracted (Fig. 1 c). For each ATP concentration, we obtained, typically, 90 trajectories (except at 4 μM ATP where 44 were obtained). From these trajectories, we calculated the mean displacement and the variance of the mean displacement over time for each ATP concentration (Fig. 2, a and b) and found that both increase linearly with time as expected. The velocities were determined from the slopes of mean-displacement time traces, yielding, for example (Fig. 2 a), a velocity of 143 $\pm$ 1 nm s^{-1} at an ATP concentration of 10 μM. The average velocities obtained at different ATP concentrations can be fit well with the Michaelis-Menten model, yielding an apparent Michaelis-Menten constant (K_m) of 42 $\pm$ 6 μM and a maximum velocity at an infinite ATP concentration (v_{max}) of 925 $\pm$ 33 nm s^{-1} (Fig. 2 c), in agreement with literature values (26,27). From the velocity, the variance of the mean displacement, and a step size of 8 nm, we determined the randomness of motility for each ATP concentration using Eq. 1 (Fig. 2 d). The values we obtained using TIRF microscopy at zero load are similar to those obtained with an optical tweezers force-clamp at a load of 1.05 pN (21). We determined that the randomness at 2 mM ATP (saturating concentration) is 0.45 $\pm$ 0.06, confirming that at saturating ATP, two or more exponential processes
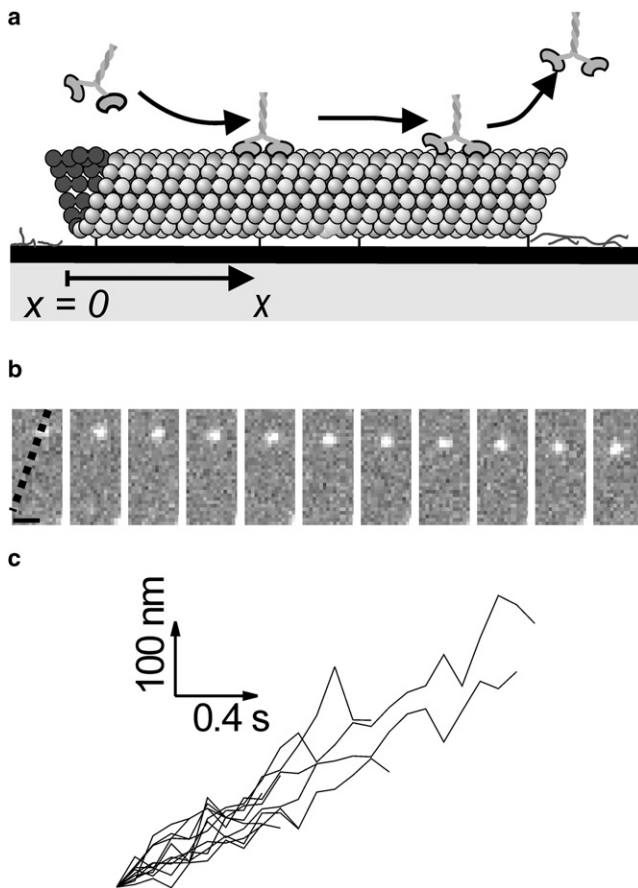
FIGURE 1 (*a*) Schematic representation of experimental assay. Labeled MTs are fixed to the surface, and labeled Kinesin-1 and ATP are added to the solution. The surface is blocked to prevent nonspecific kinesin binding. MTs and motors are visualized using TIRF microscopy. (*b*) Several frames from a time-lapse recording showing an individual Alexa-555-labeled Kinesin-1 (hKin560-421C) moving along a MT at 10 μM ATP (exposure time 90 ms; frames displayed are 450-ms apart). The MT position is indicated in the first frame by the dashed line; black scale bar is 1 μm. (*c*) Eleven representative single-molecule trajectories of Kinesin-1 at 10 μM ATP, obtained from stacks of images like in panel *b*.

are rate-limiting (Fig. 2 *d*) (20). At ATP concentrations near K_m, the randomness decreases slightly, suggesting that an additional process becomes rate-limiting. At concentrations below K_m, the randomness increases and becomes close to unity (0.8 $\pm$ 0.2 at 4 μM ATP), indicating that at very low ATP concentrations a single exponential process is rate-limiting, namely the binding of ATP. For comparison, we also plotted three curves that represent simple models with one ATP-dependent exponential process, representing ATP binding and with one, two, or three ATP-independent exponential processes of equal duration (*dashed lines*). The ATP-dependence of the randomness as obtained with TIRF microscopy is best explained by a model in which the kinetics of kinesin stepping are governed by two ATP-independent Poissonian processes with equal duration and a third ATP-dependent one (20). A different, more complex model for

kinesin mechanochemistry was proposed before by Block et al. (25) and consists of five states. In this model, the first (ATP-dependent) and second transitions are reversible. The three other transitions are irreversible and not equal. We adapted the model from the published version to correspond to the K_m and k_{cat} we measured for human Kinesin-1 at zero load. A comparison between this model and our data (Fig. 2 *d*) shows that this five-state model could be a good description of our measurements, although additional information (like the force dependence presented in (25)) would be required to discriminate between this five-state model and the simple three-state model presented before.

Kinesin's density profile along an MT reveals the average run length

Next, we set out to determine the run length of our Kinesin-1 construct. The kinesin motility traces we used above are not well suited for this purpose, since photobleaching severely limited the observed length of the runs. We performed single-molecule measurements with longer integration times and lower excitation intensity and estimate a run length of 950 $\pm$ 100 nm after correction for photobleaching (at 2 mM ATP, Fig. S1 in the Supporting Material). To circumvent both the need to correct for photobleaching and to work at the single-molecule level, we developed another approach to determine the run length. We noticed that, at kinesin concentrations too high for the clear resolving of single motors, the motor density profile on the minus-end of the MT was clearly different from that on the plus-end. Our hypothesis was that this was caused by the motors' finite run length. In Fig. 3 *a*, a TIRF microscopy image (integration time ~3 min) is shown of a Kinesin-1 coated MT. In this experiment, the Alexa-555-labeled hKin391-T217C concentration was 25 times higher than with the single-molecule measurements, and the ATP concentration was saturating (2 mM). Due to the long integration time, the motility of individual kinesins is smeared out. The intensity profile along the long axis of the MT (Fig. 3 *a*) is clearly asymmetric: the intensity increases steeply, within ~350 nm on the plus-end of the MT, while it increases more gradually on the minus-end of the MT. Similar, asymmetric intensity profiles were measured for all the other MTs in the sample. If, on the other hand, the nonhydrolyzable analog AMPPNP was used instead of ATP, the intensity profiles became more symmetric and the intensity rise at both ends of the MT was sharp, within 350 nm (Fig. 3 *b*). This was to be expected since, in the presence of AMPPNP, kinesin motors are fixed on the MT, the run length is zero, and therefore the intensity profile should drop sharply at both ends of the MT. The resulting intensity profile should be the convolution of a uniform distribution of kinesin along the MT and the point-spread function of our microscope. The point-spread function of our microscope is well approximated by a Gaussian with width 310 $\pm$ 10 nm. The convolution of such a Gaussian and
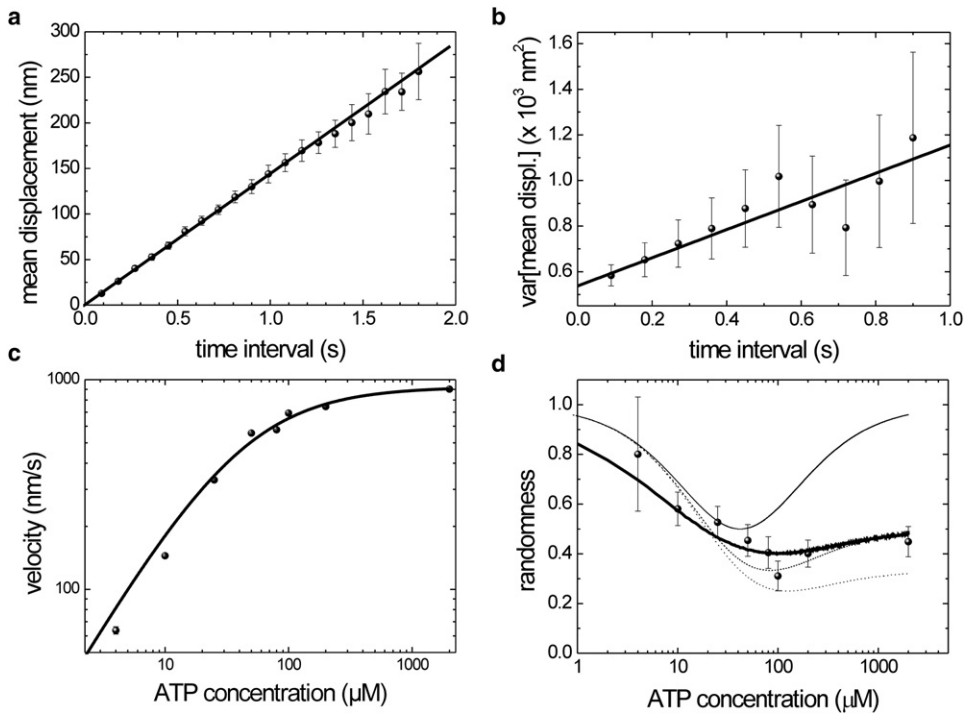
FIGURE 2 (a) Mean displacement, at 10 μM ATP, calculated for all independent time intervals in the trajectories of all runs measured. Error bars represent standard error of the mean. Solid line is a weighted fit: $MD = v\tau$ (with $v = 143 \pm 1$ nm s^{-1}). (b) Variance of the mean displacements calculated in panel A. Error bars represent the standard error of the mean. Solid line is a weighted fit to $varMD = C\tau + offset$ (offset reflects the localization uncertainty of 23 nm, the slope $C = 620 \pm 80$ nm^2 s^{-1}). (c) Average velocity of Kinesin-1 at different ATP concentrations (calculated from a weighted fit of the mean displacement). Data is fitted with the Michaelis-Menten model $v = v_{max}$ [ATP]/([ATP] + K_m), yielding $K_m = 42 \pm 6$ μM and $v_{max} = 925 \pm 33$ nm s^{-1}. (d) Randomness as a function of ATP concentration, calculated from a weighted fit of the time trace of the variance from panel B, an 8-nm step size and the average velocity (Eq. 1). The three thin black curves are models of the ATP dependence of the randomness assuming one ($\chi^2 = 132.41$), two ($\chi^2 = 7.15$), or three ($\chi^2 = 26.19$) ATP-independent exponential processes (thin solid, thin dashed, and thin dotted curve, respectively). The randomness is best described by a model with two ATP-independent exponential processes. The thick, solid curve represents a complex, five-state model with the first two reversible transitions followed by three irreversible transitions ($k_{on} = 3.5$ μM^{-1} s^{-1}, $k_{off} = 236$ s^{-1}, $k_2 = 2573$ s^{-1}, $k_{-2} = 7$ s^{-1}, $k_3 = 1084$ s^{-1}; and $k_4 = 325$ s^{-1}, $k_5 = 223$ s^{-1}, and $\chi^2 = 4.00$).

a step function (resulting in an error function) provides a good description of the AMPPNP data (Fig. 3 b), indeed indicating that the kinesin density is constant along a MT and drops sharply to zero beyond the length of the MT. This is in contrast to the gradual fluorescence incline that is observed on one side of kinesin-coated MTs in the presence of ATP.

To understand, quantitatively, the intensity profile in the presence of ATP, we modeled the density profile of kinesin binding to a MT from solution and walking unidirectionally along it. Assuming equilibrium between MT-bound kinesins and kinesin in solution (i.e., the average number of kinesins detaching equals the average number of kinesin attaching to a MT) and assuming that the kinesin binding sites on the MT do not saturate (the motor concentration should be adjusted accordingly), a steady-state differential equation can be expressed as

$$v\frac{dn(x)}{dx} = kn_0 - k'n(x) - k'_{bleach}n(x), \qquad (2)$$

where v is kinesin's velocity, n_0 its concentration in solution, k the attachment rate, k' the detachment rate of MT-bound motors, k'_{bleach} the rate of photobleaching, and $n(x)$ the kinesin number on the MT as a function of the position x. The minus-end of the MT is the $x = 0$ position (Fig. 1 a). Here we assume a homogenous field of illumination, such that the rate of photobleaching is position-independent. To solve

this differential equation, we set the kinesin number on the minus-end of the MT to zero and find

$$n(x) = \frac{l_{app}kn_0}{v}\left(1 - e^{-x/l_{app}}\right), \qquad (3)$$

where l_{app} is the apparent run length, defined as (with l the real run length)

$$l_{app} = \frac{v}{k' + k'_{bleach}} = \frac{l}{1 + \frac{k'_{bleach}}{k'}}. \qquad (4)$$

The intensity profile on the minus-end of the MT is described by Eq. 3. However, it does not describe the intensity drop-off at the plus-end of the MT. To fully describe the intensity profile along the entire length of the MT, Eq. 3 has to be convoluted with the point-spread function (approximated by a Gaussian), yielding fit equations as described in the Supporting Material. The resulting fit of the entire intensity profile along the MT (Fig. 3 a) yields an apparent run length of 908 nm. The apparent run lengths were obtained from fitting the intensity profiles of 32 MTs observed under the same conditions from a Gaussian distribution, with an average of 1070 $\pm$ 30 nm (mean $\pm$ standard error) (Fig. 3 c). This apparent run length could, in principle, deviate from the real one (as described by Eq. 4), if the rate of detachment was not substantially larger than the rate of photobleaching.
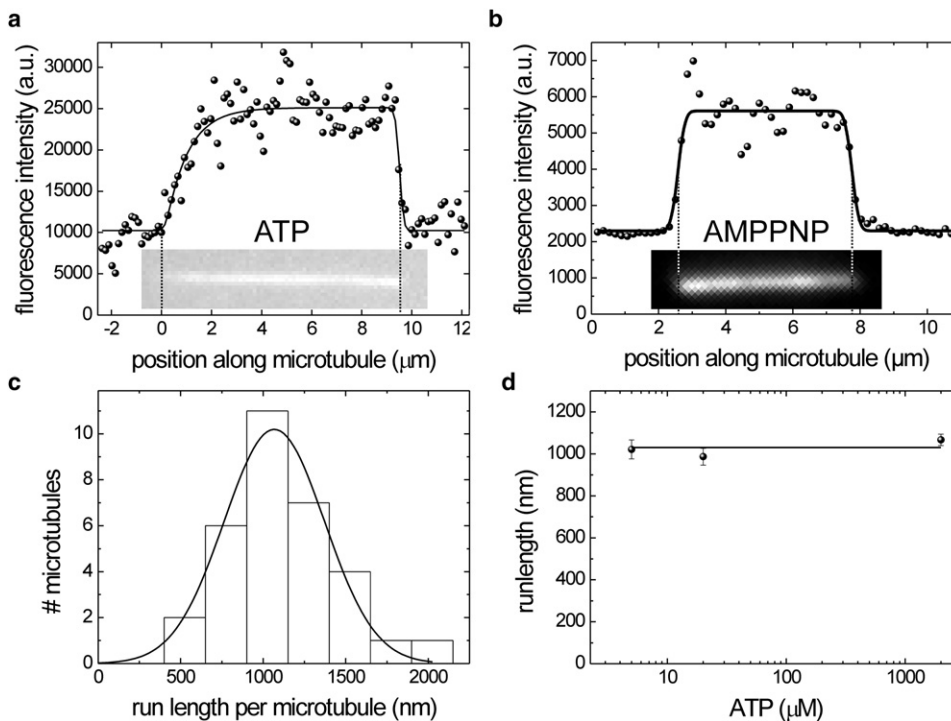
FIGURE 3 (a) Time-integrated intensity profile of a MT with moving Alexa-555 labeled Kinesin-1 (hKin391-T217C). The corresponding integrated image of the MT is shown below the profile. The profile was determined summing over the width of the image of the microtubule (three pixels). This profile was constructed by integrating 200 frames with 1-s exposure time each. The solid line represents a fit of Eq. S1 to the data points with the same position range as the fit curve. Fit parameters are $A = 7261$, $d = 9670$ nm, $x_0 = 65$ nm, $r = 290$ nm, $l_{app} = 908$ nm, and $B = 10{,}220$. (b) Time-integrated intensity profile of an MT decorated with AMPPNP fixed kinesins. The MT is shown below the profile, and was illuminated with a threefold higher intensity than the MT in panel a. Each point in the profile is calculated in the same manner as described in panel a, the z scale has the same relative scale, the integration was 1 s, and 30 frames were summed. The solid line represents a fit of a convolution of a block function with a Gaussian with a fixed width, $A(Erf(2(x-x_{c1})/FWHM)) + Erf(2(x-x_{c2})/FWHM)) + I_o$ (Erf being the error function, and x_{c1} and x_{c2} are the locations of the MT ends). Fit values are $A = 3310$, $x_{c1} = 2576$ nm, $x_{c2} = 7759$ nm, and $I_0 = 2298$. The FWHM was set to 310 nm. (c) Distribution of run lengths obtained from individual MTs decorated with moving Kinesin-1 at an ATP concentration of 2 mM. The solid line represents a Gaussian fit with a center position at 1070 ± 30 nm. (d) Average run length of Kinesin-1 at different ATP concentrations. Averages and their mean $\pm$ standard error are determined from the Gaussian fit on the distribution of average run lengths of single MTs (2 mM, 32 MTs; 20 μM, 25 MTs; and 5 μM, 18 MTs). The solid line, to guide the eye, represents the average of the three values 1030 ± 40 nm.

We determined that under our experimental conditions the rate of photobleaching is <0.001 s^{-1}, by measuring the rate of single fluorophore bleaching on MT-bound kinesins in the presence of 1 mM AMPPNP (data not shown). The average detachment rate of the motor was more than an order-of-magnitude larger, 0.05 s^{-1} (v/l, at the lowest velocity measured: $v = 60$ nm/s at 5 μM ATP, see below), indicating that photobleaching did not affect our determination of the run length, within the uncertainty of the measurements. The run length determined from the kinesin density on the minus-end of the MT, 1070 ± 30 nm, is in good agreement with the value we determined in the traditional way (Fig. S1) and values reported before for similar Kinesin-1 constructs at saturating ATP concentrations (16,17,26).

The run length of kinesin at low ATP concentrations

Next, we set out to measure the run length of our Kinesin-1 construct at lower ATP concentrations. At low ATP concentrations, kinesin spends an appreciable amount of its total cycle time in an ATP waiting state, an amount that increases with decreasing ATP concentration. If the ATP waiting state is a weakly-bound state with a relatively high probability for detachment, one would expect the run length to be ATP concentration-dependent. If, on the other hand, the ATP

waiting state were to be a strongly bound state, with a low probability of detachment (compared to the other states in the cycle), the run length would not be affected by the concentration of ATP. Experimental determinations of the ATP-dependence of the run length have yielded conflicting results (19,28), but have been used for modeling of Kinesin-1 motility (28,29). When we apply the intensity profile approach to samples with a low ATP concentration, we observe that the run length is independent of ATP concentration (Fig. 3 d), confirming the results of an earlier report (19). Our results are consistent with models with an ATP-waiting state that is tightly MT-bound and has a very low off-rate (30).

DISCUSSION AND CONCLUSIONS

Single-molecule fluorescence microscopy is a well-established technique to measure the motility of single, fluorescently labeled motor proteins such as kinesin under biochemical conditions (ATP concentration and ionic strength) in vitro. In particular, it has been widely applied to determine the motor's velocity and run length (19,31) and it has been used to measure the step sizes of individual motor domains (11). Here we have shown that TIRF microscopy can also be used to measure the randomness of the motility. The randomness is a parameter that provides information on the stochastic nature of the

underlying motility process—in particular, the number of rate-limiting exponential processes that underlie motility.

Furthermore, we demonstrated a novel way of determining the run length of kinesin from the intensity profile of many fluorescent kinesins walking along a MT. We observed that, on the MT minus-end, the intensity increases more gradually compared to the plus-end of the MT. Indeed, the intensity increase on the minus-end follows exponential saturation, with an exponential constant equal to the run length. Run lengths have before been determined from single-molecule tracking measurements using optical tweezers (2) or fluorescence microscopy (31). The former approach can only be performed under load; the latter suffers from complications due to photobleaching. Our approach has the key advantage of providing data averaged over many motors that were obtained in a single measurement. It hardly suffers from photobleaching and does not require single-molecule observations. Our method does, however, require homogeneous illumination, a good batch of proteins (without dead motors that remain stuck on the MT), and a run length that is at least as long as the point-spread function of the instrument, ~300 nm.

We have shown here that TIRF microscopy, which is far less complex than other methods such as optical tweezers and is available in many labs, can be used to determine, reliably, the key motility parameters of run length, velocity, and randomness—all three as a function of ATP concentration. An additional advantage of TIRF microscopy is that, by using this method, no load is applied to the motors. We envision that the approaches presented here can be applied by many labs to various other motor proteins from the kinesin, and other super-families that still remain to be characterized.

Using these approaches, we have shown here that the run length of Kinesin-1 is 1070 ± 30 nm, independent of ATP concentrations. Our observations, which are not hampered by the effects of photobleaching, settle a discrepancy between previous experimental and modeling studies (19,28,29). In addition, we have measured the ATP-dependence of the randomness, at zero load. Our results show that the rate of Kinesin-1 is limited by two or more exponentially distributed processes at high ATP concentrations, but that an additional, ATP-dependent process becomes the sole rate-limiting process at low ATP concentrations. These results will be of importance for a detailed understanding of Kinesin-1's mechanism and kinetics.

SUPPORTING MATERIAL

One figure and one equation are available at http://www.biophysj.org/biophysj/supplemental/S0006-3495(09)01316-2.

REFERENCES

1. Vale, R. D., T. S. Reese, and M. P. Sheetz. 1985. Identification of a novel force-generating protein, kinesin, involved in microtubule-based motility. *Cell.* 42:39–50.

2. Svoboda, K., C. F. Schmidt, B. J. Schnapp, and S. M. Block. 1993. Direct observation of kinesin stepping by optical trapping interferometry. *Nature.* 365:721–727.

3. Schnitzer, M. J., and S. M. Block. 1997. Kinesin hydrolyzes one ATP per 8-nm step. *Nature.* 388:386–390.

4. Howard, J., A. J. Hudspeth, and R. D. Vale. 1989. Movement of microtubules by single kinesin molecules. *Nature.* 342:154–158.

5. Carter, N. J., and R. A. Cross. 2006. Kinesin's moonwalk. *Curr. Opin. Cell Biol.* 18:61–67.

6. Cappello, G., M. Badoual, A. Ott, J. Prost, and L. Busoni. 2003. Kinesin motion in the absence of external forces characterized by interference total internal reflection microscopy. *Phys. Rev. E Stat. Nonlin. Soft Matter Phys.* 68:021907.

7. Busoni, L., A. Dupont, C. Symonds, J. Prost, and G. Cappello. 2006. Short time investigation of the *Neurospora* kinesin step. *J. Phys. Condens. Matter.* 18:S1957–S1966.

8. Larson, D. R., R. Thompson, and W. W. Webb. 2002. Precise nanometer localization analysis for individual fluorescent probes. *Biophys. J.* 82:45A.

9. Schmidt, T., G. J. Schutz, W. Baumgartner, H. J. Gruber, and H. Schindler. 1996. Imaging of single molecule diffusion. *Proc. Natl. Acad. Sci. USA.* 93:2926–2929.

10. Yildiz, A., J. N. Forkey, S. A. McKinney, T. Ha, Y. E. Goldman, et al. 2003. Myosin V walks hand-over-hand: single fluorophore imaging with 1.5-nm localization. *Science.* 300:2061–2065.

11. Yildiz, A., M. Tomishige, R. D. Vale, and P. R. Selvin. 2004. Kinesin walks hand-over-hand. *Science.* 303:676–678.

12. Asbury, C. L., A. N. Fehr, and S. M. Block. 2003. Kinesin moves by an asymmetric hand-over-hand mechanism. *Science.* 302:2130–2134.

13. Kaseda, K., H. Higuchi, and K. Hirose. 2003. Alternate fast and slow stepping of a heterodimeric kinesin molecule. *Nat. Cell Biol.* 5:1079–1082.

14. Kapitein, L. C., E. J. G. Peterman, B. H. Kwok, J. H. Kim, T. M. Kapoor, et al. 2005. The bipolar mitotic kinesin Eg5 moves on both microtubules that it crosslinks. *Nature.* 435:114–118.

15. Reck-Peterson, S. L., A. Yildiz, A. P. Carter, A. Gennerich, N. Zhang, et al. 2006. Single-molecule analysis of dynein processivity and stepping behavior. *Cell.* 126:335–348.

16. Seitz, A., and T. Surrey. 2006. Processive movement of single kinesins on crowded microtubules visualized using quantum dots. *EMBO J.* 25:267–277.

17. Thorn, K. S., J. A. Ubersax, and R. D. Vale. 2000. Engineering the processive run length of the kinesin motor. *J. Cell Biol.* 151:1093–1100.

18. Gelles, J., B. J. Schnapp, and M. P. Sheetz. 1988. Tracking kinesin-driven movements with nanometer-scale precision. *Nature.* 331:450–453.

19. Yajima, J., M. C. Alonso, R. A. Cross, and Y. Y. Toyoshima. 2002. Direct long-term observation of kinesin processivity at low load. *Curr. Biol.* 12:301–306.

20. Svoboda, K., P. P. Mitra, and S. M. Block. 1994. Fluctuation analysis of motor protein movement and single enzyme-kinetics. *Proc. Natl. Acad. Sci. USA.* 91:11782–11786.

21. Visscher, K., M. J. Schnitzer, and S. M. Block. 1999. Single kinesin molecules studied with a molecular force clamp. *Nature.* 400:184–189.

22. Verbrugge, S., L. C. Kapitein, and E. J. G. Peterman. 2007. Kinesin moving through the spotlight: single-motor fluorescence microscopy with submillisecond time resolution. *Biophys. J.* 92:2536–2545.

23. Kwok, B. H., L. C. Kapitein, J. H. Kim, E. J. G. Peterman, C. F. Schmidt, et al. 2006. Allosteric inhibition of kinesin-5 modulates its processive directional motility. *Nat. Chem. Biol.* 2:480–485.

24. Saxton, M. J. 1997. Single-particle tracking: the distribution of diffusion coefficients. *Biophys. J.* 72:1744–1753.

25. Block, S. M., C. L. Asbury, J. W. Shaevitz, and M. J. Lang. 2003. Probing the kinesin reaction cycle with a 2D optical force clamp. *Proc. Natl. Acad. Sci. USA.* 100:2351–2356.

26. Coy, D. L., M. Wagenbach, and J. Howard. 1999. Kinesin takes one 8-nm step for each ATP that it hydrolyzes. *J. Biol. Chem.* 274:3667–3671.

27. Nishiyama, M., H. Higuchi, and T. Yanagida. 2002. Chemomechanical coupling of the forward and backward steps of single kinesin molecules. *Nat. Cell Biol.* 4:790–797.

28. Schnitzer, M. J., K. Visscher, and S. M. Block. 2000. Force production by single kinesin motors. *Nat. Cell Biol.* 2:718–723.

29. Fisher, M. E., and A. B. Kolomeisky. 2001. Simple mechanochemistry describes the dynamics of kinesin molecules. *Proc. Natl. Acad. Sci. USA.* 98:7748–7753.

30. Uemura, S., K. Kawaguchi, J. Yajima, M. Edamatsu, Y. Y. Toyoshima, et al. 2002. Kinesin-microtubule binding depends on both nucleotide state and loading direction. *Proc. Natl. Acad. Sci. USA.* 99:5977–5981.

31. Vale, R. D., T. Funatsu, D. W. Pierce, L. Romberg, Y. Harada, et al. 1996. Direct observation of single kinesin molecules moving along microtubules. *Nature.* 380:451–453.